Hindawi Publishing Corporation
Journal of Nanomaterials
Volume 2015, Article ID 761286, 8 pages
http://dx.doi.org/10.1155/2015/761286

*Research Article*

# Superhydrophobicity, Microwave Absorbing Property of $NiFe_2O_4$/Wood Hybrids under Harsh Conditions

**Qiufang Yao,[1] Chunde Jin,[1,2] Huanhuan Zheng,[1] Zhongqing Ma,[1] and Qingfeng Sun[1,2]**

[1]*School of Engineering, Zhejiang A&F University, Lin'an 311300, China*
[2]*Key Laboratory of Wood Science and Technology, Lin'an 311300, China*

Correspondence should be addressed to Qingfeng Sun; qfsun@zafu.edu.cn

Received 20 July 2015; Accepted 8 October 2015

Academic Editor: Youssef Habibi



Magnetic $NiFe_2O_4$ nanoparticles were successfully deposited on the wood surface via a hydrothermal process at 70°C. The surface of the as-prepared magnetic $NiFe_2O_4$/wood hybrids (MWHs) was covered by spherical-like $NiFe_2O_4$ particles with an average size of 50 nm. MWH exhibited the thermostability, microwave absorbability, and superparamagnetism with saturation magnetization ($M_s$) of 1.79 emu·g$^{-1}$. With further modification by 1H,1H,2H,2H-perfluorodecyltrimethoxysilane (FAS-17), MWH expressed superhydrophobic performances with a water contact angle of 158°. Its superparamagnetism stably remained under harsh conditions after chemical solutions corrosion and physical frozen test.

## 1. Introduction

With superior properties such as improved thermal, mechanical, and dimensional stability, inorganic nanoparticles/wood hybrids have attracted significant interest in recent years [1, 2]. Only a thin coating of inorganic nanoparticles deposited on wood surface has been demonstrated to lower the rate of moisture sorption [3]. This is attributed to synergistic effects resulting from the physical or chemical interactions between the inorganic and wood components. Simultaneously, some interesting properties, such as UV resistance, fire resistance, or superhydrophobic performances, were also granted to wood by surface deposition of nanometer-sized inorganic particles, such as $SiO_2$ [4], $TiO_2$ [5], and ZnO [6]. However, there were rare researches focused on the exploration of magnetic nanoparticles deposited on wood surface. The wood embedded with magnetic properties would be a potential for indoor electromagnetic wave absorber, antistatic property, and heavy metal adsorption, which may be a multifunctional material with woody and magnetic characteristics [7–9].

Herein, the magnetic wood was produced successfully by precipitated $NiFe_2O_4$ nanoparticles on the wood surface. The as-prepared products were characterized by scanning electron microscopy (SEM), high resolution transmission electron microscopy (HRTEM), X-ray diffraction (XRD), a thermal analyzer (TGA, SDT Q600), and vibrating sample magnetometer (VSM). Interestingly, the prepared magnetic wood also showed microwave absorption. Then the surface should be subsequently modified with a layer FAS-17 to obtain superhydrophobicity. Moreover, the superhydrophobic magnetic wood specimens were evaluated as well in harsh condition.

## 2. Material and Methods

*2.1. Materials.* Each piece of poplar wood (*Populus ussuriensis* Kom.) has a size of 20 mm × 20 mm × 2 mm. Then the wood specimens were ultrasonically rinsed in acetone and deionized water for several times and oven dried at 105°C until stabilization of their mass before determination of their anhydrous weights. All chemicals were supplied by Aladdin Industrial Co. and used as received.

*2.2. Fabrication of Magnetic $NiFe_2O_4$/Wood Hybrids (MWHs) via a Hydrothermal Process.* MWH was synthesized as follows: nickel chloride (0.5 M) and ferric chloride (1 M) were

dissolved in distilled water in a 100 mL glass container at room temperature under vigorously magnetic stirring for 20 min. And then the solution was transferred into a Teflon container (70%). Wood specimens were subsequently placed into the above reaction solution and the autoclave was sealed and maintained at 70°C for 3 h and then aqueous hydrazine solutions (40 wt.%) with ammonia solution (28 wt.%) at appropriate amounts were added dropwise to adjust the pH value to 10. Further continuing hydrothermal process, the system was maintained at 70°C for 3 h and then cooled to room temperature naturally. After that, the wood specimens were removed from the solutions and ultrasonically rinsed in deionized water for 20 min and subsequently vacuum dried at 60°C for 48 h. For comparative studies, the control wood specimens (CW) were also gathered.

*2.3. Fabrication of the Superhydrophobic Magnetic $NiFe_2O_4$/Wood Hybrids (SMWHs).* MWH was immersed in the methanol of FAS-17 with the volumetric concentration of 1% for 24 h at room temperature. Subsequently, the specimens were washed with ethanol to remove any residual chemicals and allowed to dry in air at room temperature and then dried at 60°C for 48 h.

*2.4. Characterizations.* The surface morphologies of the specimens were characterized by the scanning electron microscopy (SEM, FEI, Quanta 200, USA) and transmission electron microscope (TEM, FEI, Tecnai G20, USA). Atomic force microscopy (AFM) image was obtained using a Multimode Nanoscope IIIa controller (AFM, Veeco Inc., USA) with a silicon tip operated in a tapping mode to characterize the surface morphology and the thickness. Crystalline structures of the specimens were identified by the X-ray diffraction technique (XRD, Rigaku D/MAX 2200, Japan) operating with Cu K$\alpha$ radiation ($\lambda$ = 1.5418 Å) at a scan rate ($2\theta$) of 2° $min^{-1}$ and the accelerating voltage of 40 kV and the applied current of 30 mA ranging from 10° to 70°. The magnetic properties of the composites were measured by vibrating sample magnetometer (VSM LakeShore Model 7404, California, USA) at 300 K. The contact angle analyzer (Pereach Co. JC2000C, China) at ambient temperature with a droplet volume of 5 $\mu$L was employed to measure the contact angles (CAs) of the specimens. An average of the five measurements taken at different positions on each sample was applied to calculate the final CA value. The thermal performances of the magnetic wood composites were examined using a thermal analyzer (TGA, SDT Q600, USA) in the temperature range from room temperature up to 800°C at a heating rate of 10°C/min with nitrogen. The relative permeability and permittivity were obtained on a network analyzer (Agilent N5244A PNA-X, California, USA) in the frequency range of 2–18 GHz for the calculation of reflection loss (RL) by the coaxial reflection/transmission method based on NRW method. The sample containing composite materials and paraffin wax with the mass ratio of 1 : 2 was pressed into toroidal-shaped samples ($\Phi_{out}$ = 7.00 mm, $\Phi_{in}$ = 3.04 mm, and thickness = 2 mm) for microwave measurement. The simulated reflection loss (RL) was calculated from the measured parameters according to the transmission line theory.

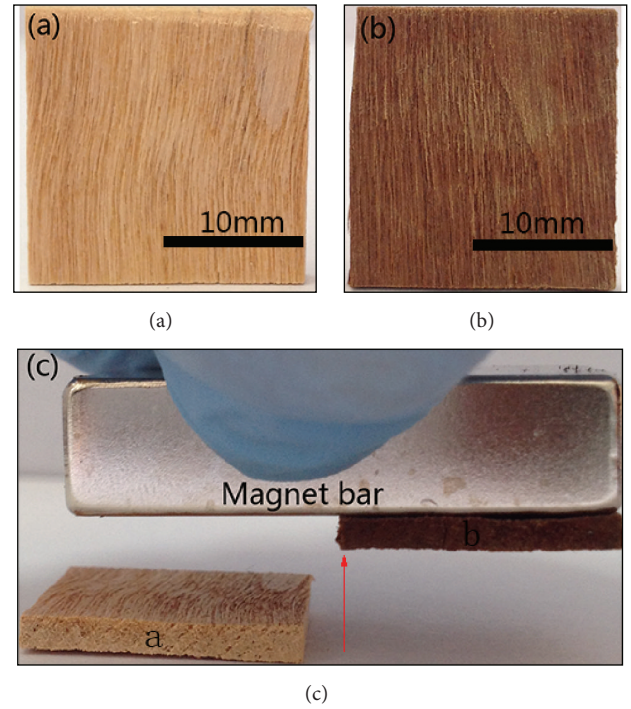


Figure 1: Figure 1: Surface images of CW (a) and MWH (b), (c) MWH attracted by a magnet bar.

*2.5. Evaluation of the Stability of SMWH.* On the one hand, SMWH specimens were fixed and immersed into corrosive solutions (for acid: a hydrochloric acid solution of pH = 1; considering alkaline: a sodium hydroxide solution of pH = 14; for salt: a sodium chloride solution (3 M)) for 12 h at room temperature, respectively. On the other hand, SMWH was frozen at −35°C for 12 h. Subsequently, all of these specimens were removed, ultrasonically rinsed, vacuum dried, and finally characterized by the contact angle analyzer and a vibrating sample magnetometer (VSM).

## 3. Results and Discussion

Figure 1 shows the camera images of CW and MWH, the magnetic property of MWH, respectively. Compared to CW (Figure 1(a)), MWH in Figure 1(b) had certain color appearance changes with brown, which illustrated something grown on CW surface. In Figure 1(c), MWH could be smoothly moved to a magnet while CW remained motionless, which confirmed that the magnetic particles might be deposited on the wood surface.

Figure 2 shows XRD patterns of CW, MWH, and pure $NiFe_2O_4$, respectively. For CW, the diffraction peaks at about 16° and 22° were attributed to the typical reflection planes (101) and (002) of wood cellulose I. For MWH, however, new sharp peaks at $2\theta$ of 30.5°, 35.8°, 43.5°, 53.8°, 57.4°, and 63.1° ascribed to the crystal planes (220), (311), (400), (422), (511), and (440) are attributed to the spinel phases of $NiFe_2O_4$ (JCPDS card number 74-2081) [10]. In addition, the disappearance of diffraction peaks of cellulose might be due to a dense thickness of $NiFe_2O_4$ nanoparticles coating

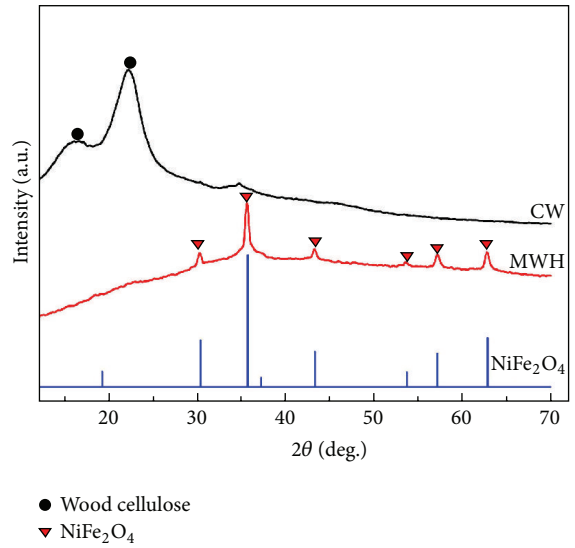


Figure 2: XRD patterns of CW, MWH, and pure $NiFe_2O_4$, respectively.

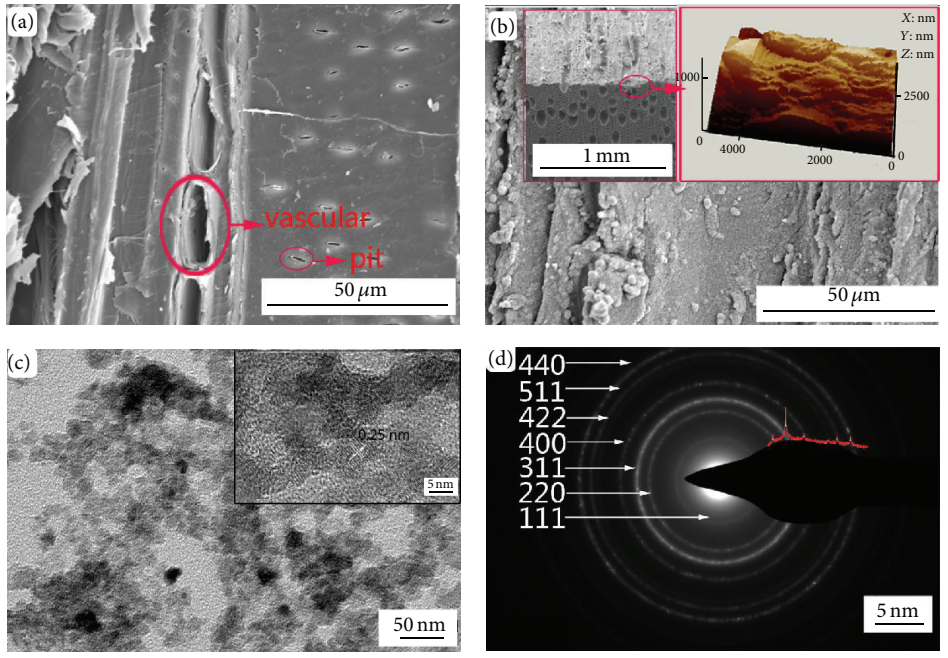


Figure 3: (a) SEM image of CW; (b) SEM image of MWH, its low magnification SEM image, and AFM (the inset); (c) TEM image and HRTEM images (the inset); (d) SAED pattern of $NiFe_2O_4$ nanoparticles.

on wood surface. The thickness would be given by the AFM pattern (Figure 3(d)). Moreover, no other peaks are observed, implying the high purity of the obtained products. Hence, $NiFe_2O_4$ nanoparticles with good crystalline were successfully grown on wood surface.

Figure 3 exhibits SEM images of CW and MWH, AFM image of MWH surface, TEM image, and the selected area electron diffraction (SAED) of the magnetic particles, respectively. In Figure 3(a), there are a considerable number of pits and vascular bundle in wood structure [11]. After the hydrothermal treatment, in Figure 3(b), the surface of CW was covered by a dense film of spherical-like $NiFe_2O_4$ particles and AFM image shows the thickness of the film was approximately 1.2 $\mu$m (the insert). Figure 3(c) shows an average diameter of spherical-like $NiFe_2O_4$ particles, which were peeled off from wood surface via a strong ultrasonic treatment with 1200 w, is about 27 nm. Specially, the inset image clearly shows the distance between two adjacent planes is measured to be 2.5 Å, corresponding to (311) planes in the spinel-structured $NiFe_2O_4$ [12]. Figure 3(d) exhibits the selected area electron diffraction (SAED) pattern acquired from $NiFe_2O_4$ particles peeled off from wood surface via

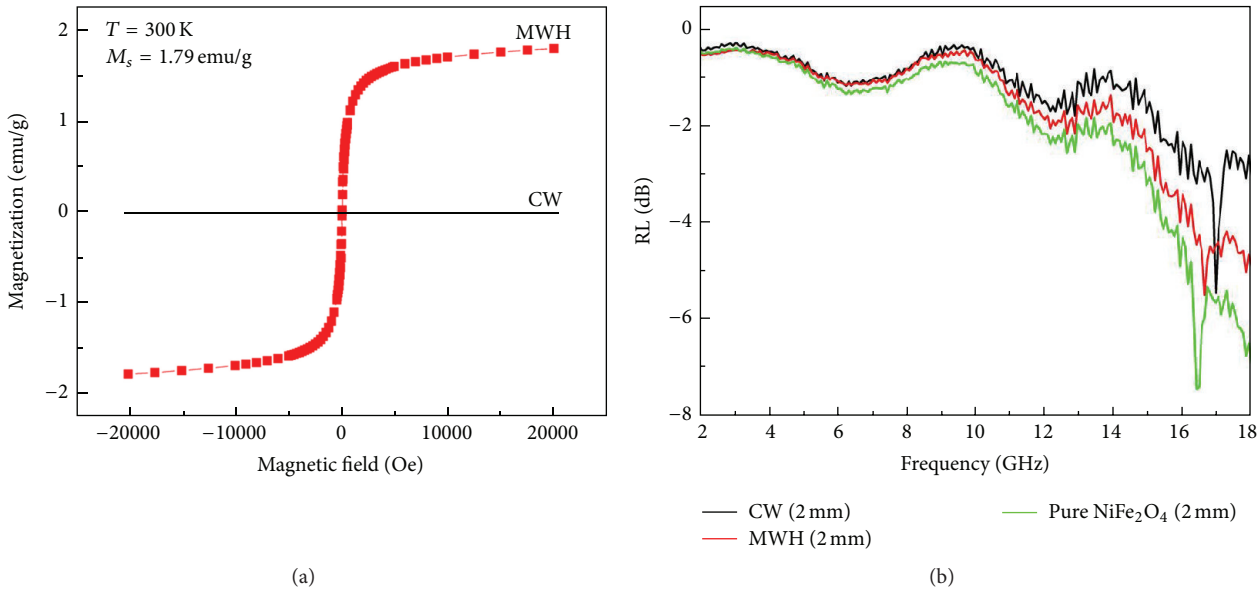


Figure 4: Magnetic hysteresis loops for CW and MWH and the reflection loss (RL) values of CW, MWH, and pure $NiFe_2O_4$ powder.

a strong ultrasonic treatment with 1200 w. It can be well indexed to (111), (220), (311), (400), (422), (511), and (440) of face centered cubic spinel structure using the SAED patterns, which is consistent with the results of XRD.

Figure 4 illustrates the magnetization versus applied magnetic field (M-H) hysteresis curves of CW and MWH examined at 300 K (Figure 4(a)) and microwave absorption properties of MWH (Figure 4(b)). In Figure 4(a), hysteresis loops can be observed, indicating that, compared with non-magnetism CW, MWH exhibited a well superparamagnetic behavior [13]. The magnetization of MWH increased with an increasing magnetic field and MWH exhibited extremely small hysteresis loops and little coercivity and the saturation magnetization ($M_s$) of MWH obtained from the hysteresis loop was 1.79 emu·$g^{-1}$.

To reveal the microwave absorption properties of the as-synthesized specimens, the reflection loss (RL) values of CW, MWH, and pure $NiFe_2O_4$ powder were calculated in the frequency range of 2–18 GHz [14]. As shown in Figure 4(b), for CW, there is one broad and sharp wave absorbing peak in the range of 2–18 GHz, and the minimum RL reached −5.8 dB at 17 GHz with the thickness of 2 mm. For $NiFe_2O_4$ sphere-like microstructures of MWH, there is also one broad and strong wave absorbing peak in the range of 2–18 GHz, and the minimum RL similarly reached −5.8 dB at 16.7 GHz with the thickness of 2 mm, which was lower than intensity of pure $NiFe_2O_4$ precursor (−7.4 dB at 16.7 GHz). The microwave absorption with RL < −5 dB almost covers the full X-band (8–12 GHz), indicating that CW and MWH provide a potential for microwave absorption.

Figure 5 shows the thermogravimetric and differential thermogravimetric analysis (TG-DTG) curves of CW and MWH with nitrogen atmosphere. In the first stage (25°C to 102°C), little weight loss (3–7%) in both specimens was observed which was attributed to the evaporation of moisture. In the second stage (102°C to 400°C), owing to pyrolysis of three main chemical components (cellulose, hemicellulose, and lignin) of wood [15], main weight loss had happened and the maximum pyrolysis rate occurred at 375°C and 361°C with weight loss reaching 70.2% for CW and 22.8% for MWH, respectively (Figure 5(b)). In the third stage (400°C to 800°C), the mass percentage of pyrolysis residues of CW was about 18.8 mass% from the TG curve (Figure 5(a)). However, for MWH, there was the second degradation of the three chemical components of wood. What is more, the maximum pyrolysis rate occurred at 570°C (Figure 5(b)) and weight loss was 16.7% at this stage. Finally, carbon residues and the magnetic nanoparticles were left with the weight of 44.89 mass% (Figure 5(a)). The reason for this phenomenon may be attributed to deposition of the magnetic $NiFe_2O_4$ particles on the wood surface. Combining strongly with magnetic particles via electrostatic attraction and van der Waals forces, thermal decomposition temperature of the wood increases partially from 350°C to 570°C and pyrolysis rate decreased nearly threefold, which effectively enhanced the thermal stability of wood timber. In summary, through chemical interaction between the magnetic nanoparticles and wood, thermostability of the wood was greatly improved.

Figure 6 presents superhydrophobic and magnetic performances of SMWH and SEM image of SMWH surface. In Figure 6(a), lots of spherical water drops kept sitting on the surface of SMWH attracted by magnetic bar and its WCA was around 158°, which stated superhydrophobic and magnetic performance of SMWH [16]. Figure 6(b) shows SEM image of the SMWH surface, whose microstructure is similar to that of the plant surface combined with wax

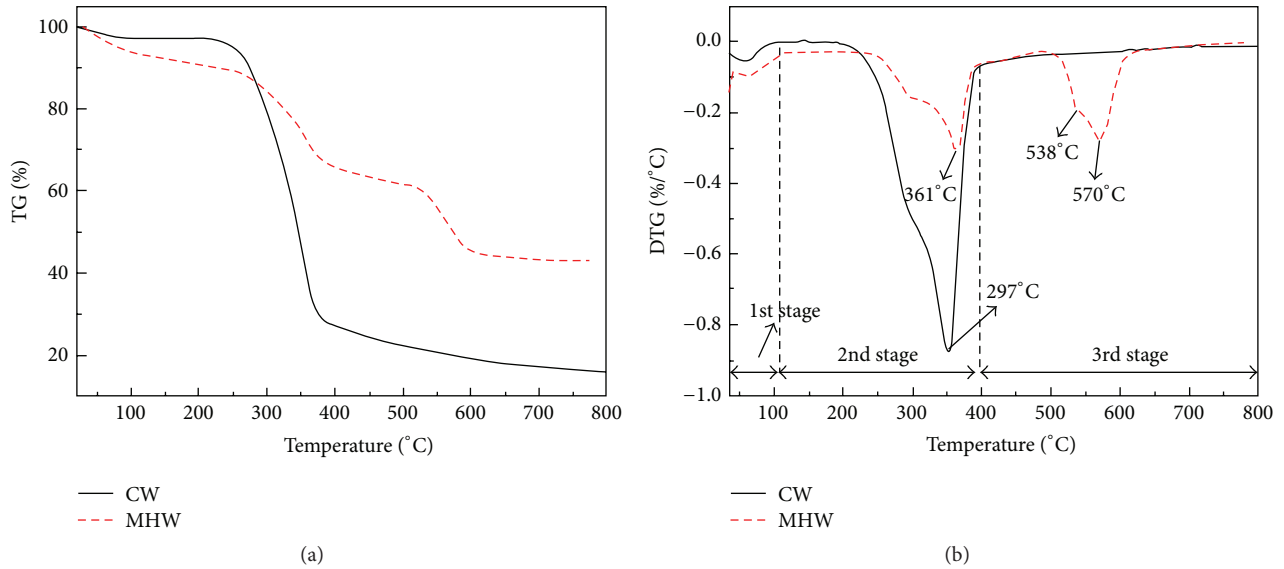


Figure 5: TG (a) and DTG (b) curves of CW and MWH.

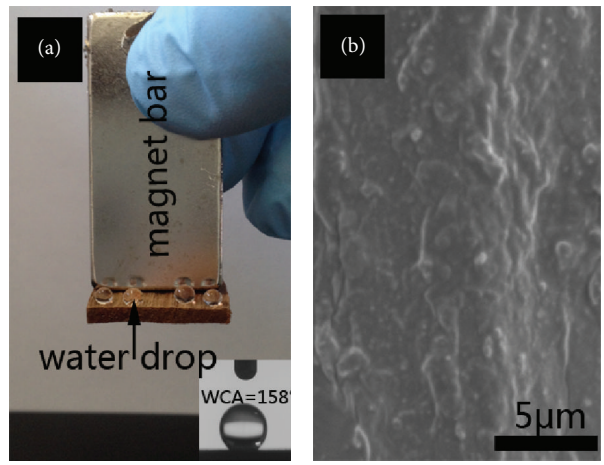


Figure 6: Superhydrophobic and magnetic performance and its WCA (the inset) of SMWH (a) and SEM image of SMWH surface (b).

crystalloids and cuticular folds. It is such microstructure and superhydrophobic long-chain alkyl groups of FAS-17 that provided a water-repellent surface [17].

Figure 7 shows that four types of common liquids, including ink, coffee, tea, and milk (Figure 7(a)), were located on the surface of CW (Figure 7(b)) and SMWH (Figure 7(c)), respectively. These spherical drops kept sitting on SMWH. In contrast, these liquids readily spread to penetrate the inner of CW, which significantly demonstrated the stain repellency of SMWH.

Figure 8 shows the stability tests of SMWH in corrosive solutions and low temperature by comparing the changes of their $M_s$ and CAs. SMWH specimens dealt with three kinds of corrosive solutions (pH = 1 (Figure 8(a)), pH = 14 (Figure 8(b)), and 3 M NaCl (Figure 8(c))) and were placed in frozen atmosphere (Figure 8(d)), respectively. After 12 h, SMWH specimens were moved away, washed, and dried to further characterization. Consequently, they were not corroded the $M_s$ and CAs of the specimens were no considerable changes which the values just decreased with 3–11%. It might be attributed to the close combination between spherical $NiFe_2O_4$ nanoparticles and FAS-17. As for the treatment with strong acid solution, $NiFe_2O_4$ particles covered by a layer of FAS-17 could not be dissolved to be iron ions under acid solution so that hydrophobic performances of SMWH remained stable. In summary, SMWH, a robust material with magnetic and hydrophobic properties, could be applied to construction materials outside [18].

Figure 9 shows the possible synthesis mechanism of SMWH. Firstly, in Figure 9(a), when CW was immersed into the precursor solution of Fe (III) and Ni (II) ions, the Fe (III) and Ni (II) ions and the plentiful OH groups of cellulose and hemicellulose in wood [19] reacted with each other by forming a complex transition state due to strong

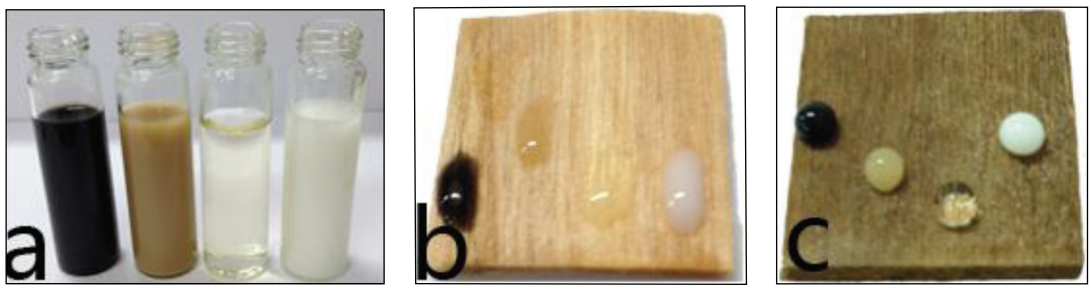


(a) (b) (c)

Figure 7: Images of daily liquids including blank ink, coffee, tea, and milk (a) droplets on the surface of CW (b) and SMWH (c).

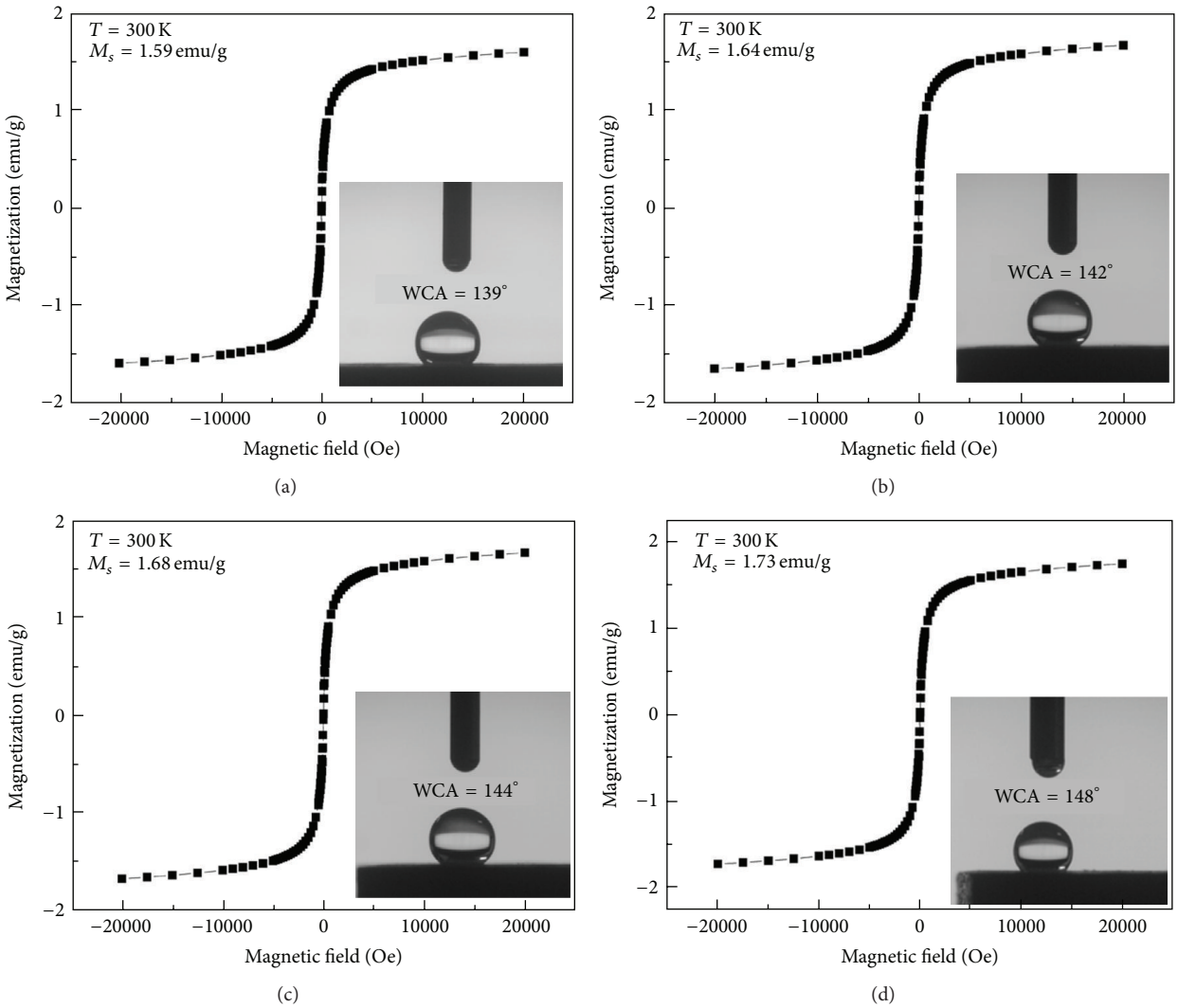


Figure 8: Magnetic hysteresis loops and WCAs of the specimens after being treated with pH = 1 (a), pH = 14 (b), and 3 M NaCl solutions (c) and frozen at −35°C (d), respectively.

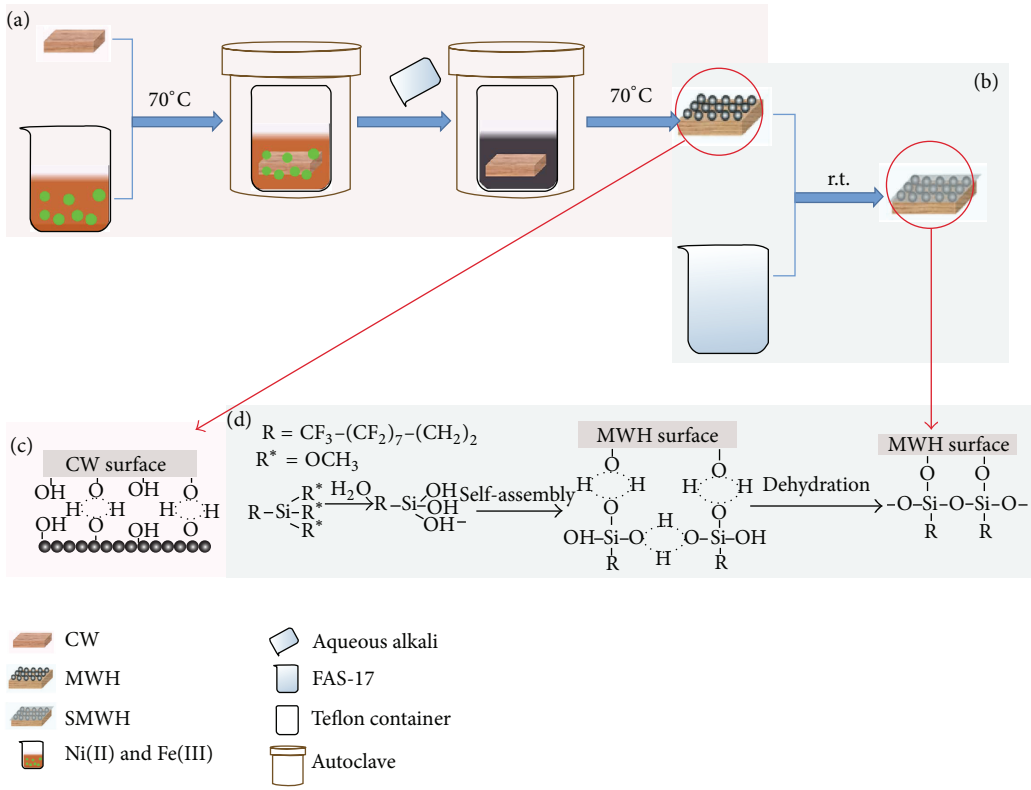


Figure 9: Possible synthesis mechanism of SMWH.

electrostatic interactions like ion-dipole interaction between iron ions and electron-rich oxygen atoms (Figure 9(c)) [20] and are followed by addition of ammonia solution, and a $NiFe_2O_4$ layer had been formed stably in situ on the CW surface. Namely, $NiFe_2O_4$ nanoparticles were successfully grown onto the wood surface; subsequently (Figure 9(b)), when the FAS-17 was added, most of the -Si-$OCH_2CH_3$ groups in FAS-17 were firstly hydrolyzed into Si-OH groups, which were attached onto the $NiFe_2O_4$ nanoparticles via the hydrogen bonds through the self-assembly process [21]. With the continuous dehydration reaction, Si-O groups with the superhydrophobic long-chain alkyl groups were formed onto both the $NiFe_2O_4$ layer and CW surfaces (Figure 9(d)). Finally, under the combined effects of $NiFe_2O_4$ nanoparticles and FAS-17, the surface became superhydrophobic. Hence, with the introduction of the hydrophobic chemical groups which can prevent the invasion of aqueous solutions such as acid, alkaline, and salt solutions, SMWH exhibited robust hydrophobic property while the magnetic particles of MWH remained the phase of $NiFe_2O_4$ rather than iron ions in these aqueous solutions.

## 4. Conclusions

In conclusion, magnetic $NiFe_2O_4$/wood hybrids were successfully fabricated and displayed superior superparamagnetism, microwave absorption properties with improved thermostability. The stable superhydrophobic magnetic $NiFe_2O_4$/wood hybrids were also prepared, which remained hydrophobic and superparamagnetic under corrosive and frozen conditions.

## Conflict of Interests

The authors declare that there is no conflict of interests regarding the publication of this paper.

## Acknowledgments

This research was supported by Zhejiang Provincial Natural Science Foundation of China under Grant no. LZ15C160002 and Scientific Research Foundation of Zhejiang A&F University (Grant no. 2014FR077).

## References

[1] I. I. Slowing, J. L. Vivero-Escoto, C.-W. Wu, and V. S.-Y. Lin, "Mesoporous silica nanoparticles as controlled release drug delivery and gene transfection carriers," *Advanced Drug Delivery Reviews*, vol. 60, no. 11, pp. 1278–1288, 2008.

[2] J. Zeng, S. Liu, J. Cai, and L. Zhang, "$TiO_2$ immobilized in cellulose matrix for photocatalytic degradation of phenol under weak UV light irradiation," *Journal of Physical Chemistry C*, vol. 114, no. 17, pp. 7806–7811, 2010.

[3] M. A. Tshabalala and L.-P. Sung, "Wood surface modification by in-situ sol-gel deposition of hybrid inorganic-organic thin films," *Journal of Coatings Technology Research*, vol. 4, no. 4, pp. 483–490, 2007.

[4] C. Mai and H. Militz, "Modification of wood with silicon compounds. Treatment systems based on organic silicon compounds—a review," *Wood Science and Technology*, vol. 37, no. 6, pp. 453–461, 2004.

[5] H. Zhang, X. Liu, Y. Li et al., "Vertically aligned nanorod-like rutile $TiO_2$ single crystal nanowire bundles with superior electron transport and photoelectrocatalytic properties," *Journal of Materials Chemistry*, vol. 22, no. 6, pp. 2465–2472, 2012.

[6] Q. Sun, Y. Lu, H. Zhang et al., "Improved UV resistance in wood through the hydrothermal growth of highly ordered ZnO nanorod arrays," *Journal of Materials Science*, vol. 47, no. 10, pp. 4457–4462, 2012.

[7] X. Sun, J. He, G. Li et al., "Laminated magnetic graphene with enhanced electromagnetic wave absorption properties," *Journal of Materials Chemistry C*, vol. 1, no. 4, pp. 765–777, 2013.

[8] X.-J. Zhang, G.-S. Wang, W.-Q. Cao et al., "Enhanced microwave absorption property of reduced graphene oxide (RGO)-$MnFe_2O_4$ nanocomposites and polyvinylidene fluoride," *ACS Applied Materials and Interfaces*, vol. 6, no. 10, pp. 7471–7478, 2014.

[9] S. Kalia, S. Kango, A. Kumar, Y. Haldorai, B. Kumari, and R. Kumar, "Magnetic polymer nanocomposites for environmental and biomedical applications," *Colloid and Polymer Science*, vol. 292, no. 9, pp. 2025–2052, 2014.

[10] M. R. Phadatare, A. B. Salunkhe, V. M. Khot, C. I. Sathish, D. S. Dhawale, and S. H. Pawar, "Thermodynamic, structural and magnetic studies of $NiFe_2O_4$ nanoparticles prepared by combustion method: effect of fuel," *Journal of Alloys and Compounds*, vol. 546, pp. 314–319, 2013.

[11] S. Jansen, B. Choat, S. Vinckier, F. Lens, P. Schols, and E. Smets, "Intervascular pit membranes with a torus in the wood of Ulmus (Ulmaceae) and related genera," *New Phytologist*, vol. 163, no. 1, pp. 51–59, 2004.

[12] M. Fu, Q. Jiao, and Y. Zhao, "Preparation of $NiFe_2O_4$ nanorod-graphene composites via an ionic liquid assisted one-step hydrothermal approach and their microwave absorbing properties," *Journal of Materials Chemistry A*, vol. 1, no. 18, pp. 5577–5586, 2013.

[13] L. Li, G. Li, R. L. Smith Jr., and H. Inomata, "Microstructural evolution and magnetic properties of $NiFe_2O_4$ nanocrystals dispersed in amorphous silica," *Chemistry of Materials*, vol. 12, no. 12, pp. 3705–3714, 2000.

[14] J. Cao, W. Fu, H. Yang et al., "Large-scale synthesis and microwave absorption enhancement of actinomorphic tubular ZnO/$CoFe_2O_4$ nanocomposites," *The Journal of Physical Chemistry B*, vol. 113, no. 14, pp. 4642–4647, 2009.

[15] H. Yang, R. Yan, H. Chen, D. H. Lee, and C. Zheng, "Characteristics of hemicellulose, cellulose and lignin pyrolysis," *Fuel*, vol. 86, no. 12-13, pp. 1781–1788, 2007.

[16] Y. Wang, Y. Shi, L. Pan et al., "Multifunctional superhydrophobic surfaces templated from innately microstructured hydrogel matrix," *Nano Letters*, vol. 14, no. 8, pp. 4803–4809, 2014.

[17] L. Jiang, Y. Zhao, and J. Zhai, "A lotus-leaf-like superhydrophobic surface: a porous microsphere/nanofiber composite film prepared by electrohydrodynamics," *Angewandte Chemie—International Edition*, vol. 43, no. 33, pp. 4338–4341, 2004.

[18] N. S. Hettiarachchy, U. Kalapathy, and D. J. Myers, "Alkali-modified soy protein with improved adhesive and hydrophobic properties," *Journal of the American Oil Chemists' Society*, vol. 72, no. 12, pp. 1461–1464, 1995.

[19] P. Gallezot, "Conversion of biomass to selected chemical products," *Chemical Society Reviews*, vol. 41, no. 4, pp. 1538–1558, 2012.

[20] J. He, T. Kunitake, and A. Nakao, "Facile in situ synthesis of noble metal nanoparticles in porous cellulose fibers," *Chemistry of Materials*, vol. 15, no. 23, pp. 4401–4406, 2003.

[21] P. Xu, X. Li, H. Yu, M. Liu, and J. Li, "Self-assembly and sensing-group graft of pre-modified CNTs on resonant microcantilevers for specific detection of volatile organic compound vapors," *Journal of Micromechanics and Microengineering*, vol. 20, no. 11, Article ID 115003, 2010.